Research paper

Design, synthesis and anticancer evaluation of novel spirobenzo[h]chromene and spirochromane derivatives with dual EGFR and B-RAF inhibitory activities

Shaimaa A. Abdelatef [a], Mohammed T. El-Saadi [a], Noha H. Amin [a], Ahmed H. Abdelazeem [a, **], Hany A. Omar [b, c], Khaled R.A. Abdellatif [d, e, *]

[a] Department of Medicinal Chemistry, Faculty of Pharmacy, Beni-Suef University, Beni-Suef, 62514, Egypt
[b] Sharjah Institute for Medical Research and College of Pharmacy, University of Sharjah, Sharjah, 27272, United Arab Emirates
[c] Department of Pharmacology, Faculty of Pharmacy, Beni-Suef University, 62514, Egypt
[d] Department of Pharmaceutical Organic Chemistry, Beni-Suef University, Beni-Suef, 62514, Egypt
[e] Pharmaceutical Sciences Department, Ibn Sina National College for Medical Studies, Jeddah 21418, Saudi Arabia

ARTICLE INFO

ABSTRACT

A novel series of spirobenzo[h]chromene and spirochromane derivatives was designed, synthesized and evaluated as potential anticancer agents against MCF-7 (human breast carcinoma), HT-29 (human colorectal adenocarcinoma) and A549 (human lung carcinoma) cell lines using MTT assay. Eight compounds 7, 8e, 13a-e and 16 showed a better anticancer activity than that of sorafenib, the multi-kinase inhibitor with IC_{50} values between 1.78 and 5.47 µM or erlotinib with IC_{50} values over 20 µM. Representative compounds 8e, 13c and 16 were selected for further mechanistic investigation via EGFR, B-RAF and tubulin polymerization assays. Compound 16 was the most potent EGFR inhibitor ($IC_{50} = 1.2$ µM), yet compounds 8e, 13c and 16 displayed moderate tubulin polymerization inhibition effects. Molecular docking studies of those compounds revealed their possible binding modes into the active sites of both EGFR and B-RAF kinases. The newly developed compounds represent a therapeutically promising approach for the treatment of different types of cancer.

© 2018 Elsevier Masson SAS. All rights reserved.

1. Introduction

Cancer has been a major public health problem worldwide with an increasing number of patients being diagnosed with cancer every year [1]. Unfortunately, the effectiveness of chemotherapy, as a principal mode of cancer treatment is limited by drug resistance, severe side effects and poor selectivity [2,3]. Thus, newly combined, multi-targeted therapies or recently, immunotherapy have been advocated [4—6]. The activation of kinases in different cell signaling pathways has been implicated in cancer cell survival, invasiveness and drug resistance [7,8]. So, targeting kinases such as epidermal growth factor receptor (EGFR) and serine/threonine kinases such as B-RAF have become one of the most intensively pursued classes of

anticancer agents [9,10]. In addition, the approval of multikinase inhibitors such as Sorafenib (Nexavar®), dual VEGFR and EGFR kinase inhibitors such as vandetanib or RAF and antiangiogenic VEGFR-PDGFRβ targeted chemotherapeutics have been adopted to produce higher potency and selectivity [11—13].

On the other hand, spirochromane has attracted significant interest as a privilege structure in the development of several bioactive compounds with a wide of biological activities [14—18]. Compounds 1 and 2 possessing spirochromanone scaffold were reported to have potent anticancer activity where they exert their action through inhibiting histone deacetylase (HDAC) enzyme, Fig. 1 [19,20]. Nevertheless, various thiosemicarbazone (TSC) and semicarbazide structures, a large group of thio/urea derivatives, have been evaluated as anticancer therapeutics over the last years, such as compounds 3, 4, Fig. 1. The conjugated N-N-S or N-N-O tridentate ligand system of thiosemicarbazides and semicarbazones, respectively, seemed essential for the anticancer activity through the inhibition of DNA synthesis produced by the modification in the reductive conversion of ribonucleotides to deoxyribonucleotides

[14,21] via reactive oxygen species generation [22–25].

Based on the aforementioned data regarding the biological significance of both spirochromane and thio/semicarbazone moieties, it was conceptualized that the tethering of these pharmacophores in one scaffold using fragment-based drug design approach would be of great interest to develop highly potent anticancer agents. Thus, we described herein, for the first time, the design and synthesis of new hybrid spiro-molecules and evaluate their anticancer potential and their dual inhibitory activities against EGFR and B-RAF kinases as a possible and valid mechanism of action for this novel class of anticancer agents.

2. Results and discussion

2.1. Chemistry

The general reactions used for the synthesis of the novel targeted spiro derivatives are outlined in Schemes 1–3. The starting material **5**, spiro[benzo[h]chromene-2,1′-cyclohexan]-4(3H)-one, was synthesized via a thermal condensation of cyclohexanone, 1′-hydroxy-2′-acetonaphthone and pyrrolidine in methanol using the reported Kabbe's multi-component reaction [26]. The furnished spirobenzo[h]chromenone compound **5** was subsequently coupled with methyl hydrazine-carbodithioate **6**, which was prepared by the reaction of hydrazine hydrate with carbon disulfide and potassium hydroxide followed by treating with methyl iodide at 10 °C, affording intermediate **7** in a quantitative yield [27]. The final targeted thiosemicarbazide compounds **8a-f** were obtained upon the displacement of the S-methyl group through the condensation of the intermediate **6** with respective amines in isopropanol with reflux for 48 h till the evolution of methyl mercaptan ceased. Meanwhile, various substituted phenyl isocyanates were reacted with hydrazine hydrate in ethanol at 0 °C to provide the phenyl-semicarbazides **9a-c** which in turn were coupled with the starting spirobenzo[h]- chromenone material **5** in the presence of TFA to afford the final targeted semicarbazide compounds **10a-c** in good yields, Scheme 1. All Postulated structures of the final spiro compounds were fully confirmed using NMR, HRMS and elemental analysis. The ^{1}H NMR spectrum of thiosemicarbazide derivative **8a**, as a representative example of the first series, revealed the absence of the S-CH$_3$ singlet peak at δ 2.68 (s, 3H) and appearance of a singlet one with two protons integration at δ 2.96 assigned to methylene protons (CH$_2$C=N) of spirobenzo[h]chromenone scaffold and a triplet signal at δ 3.84 with four protons integration

corresponding to the two methylene groups attached to the nitrogen atom of piperidine moiety. Moreover, the ^{13}C NMR spectrum of **8a** showed the appearance of a characteristic peak at δ 182.55 assigned to thiocarbonyl group and another peak at 56.51 attributed to the two methylene groups attached to the nitrogen atom of piperidine moiety. The structure of **8a** was also confirmed by HRMS where a molecular ion peak at m/z 408.1487 [M+H]$^+$ was detected, which was consistent with the molecular formula C$_{24}$H$_{29}$N$_3$OS of the targeted product.

Furthermore, the synthesis of final semicarbazide derivatives **13a-e** were carried out as depicted in Scheme 2. The spirochromanone starting materials **11a,b** were prepared using the same methodology of Kabbe's reaction through refluxing cyclohexanone or cycloheptanone with 2-hydroxyacetophenone and pyrrolidine in methanol to give the intermediates **11a** and **11b**, respectively. The spirochromanone starting materials **11a** and **11b** were reacted with hydrazine hydrate in ethanol at room temperature affording the corresponding hydrazone derivatives **12a** and **12b** which were coupled directly, without separation, with various phenylisocyanates to furnish the final targeted semicarbazide compounds **13a-e**. The structure of semicarbazide derivative **13b** was taken as an example for this series, which was verified by ^{1}H NMR spectrum that showed two singlet peaks at δ 2.80 and 2.27 assigned to the methylene and methyl groups, respectively. ^{13}C NMR spectrum revealed the appearance of some characteristic peaks at δ 154.40, 56.52 and 20.86 corresponding to carbonyl, methylene (CH$_2$—C=N) and methyl groups, respectively. HRMS showed a molecular ion peak at 364.2045 which was in agreement with the molecular formula C$_{22}$H$_{25}$N$_3$O$_2$ of compound **13b**.

Finally, the final hydrazide compounds **15-17** were prepared using the synthetic pathway showed in Scheme 3. The previous prepared spirobenzo[h]chromenone starting material **5** was allowed to react with hydrazine hydrate, in a similar manner to **11a,b** in ethanol with stirring at room temperature to give the respective hydrazone intermediate **14** which in turn was refluxed directly in glacial acetic acid with phthalic anhydride and isatin in presence of anhydrous sodium acetate to afford the final compounds **15** and **17**, respectively and with adamantyl carbonyl chloride in the presence of triethylamine to furnish the final compound **16** in a good yield. The structures of compounds **15-17** were confirmed by ^{1}H NMR and HRMS where molecular ion peaks at m/z 411.1680, 443.2698 and 410.1933 were obtained and they were found to be consistent with the exact molecular weights of **15-17**, respectively.
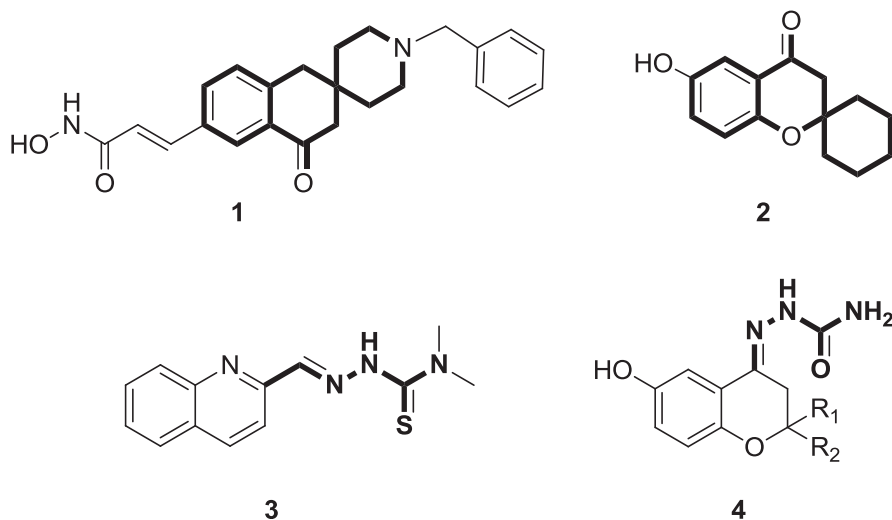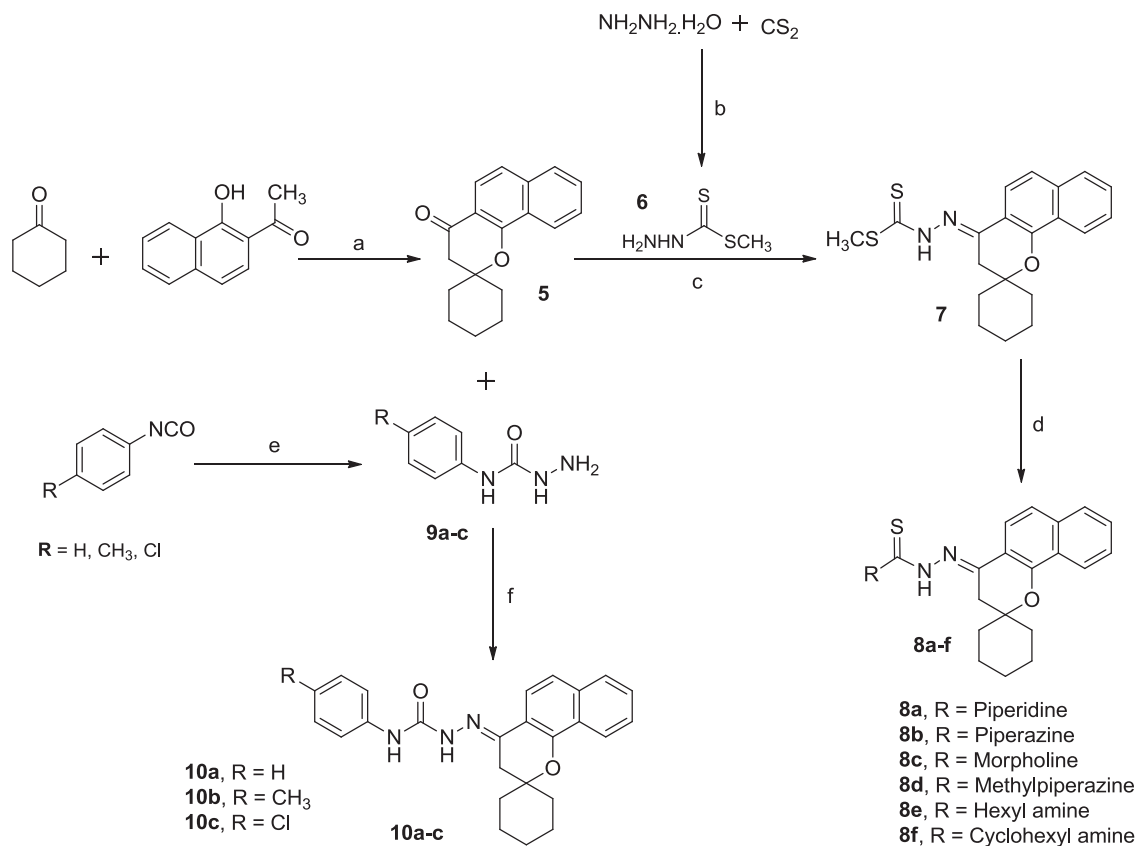

Fig. 1. Some reported spiroheterocyclic (**1** and **2**), thiosemicarbazone (**3**) and semicarbazones (**4**) derivatives with anticancer activity.

Scheme 1. Reagents and Reaction Conditions: a) Pyrrolidine, MeOH, reflux, 12 h; b) i. KOH, i-PrOH/H₂O, 0 °C, 2 h, ii. CH₃I, 0 °C, 2 h; c) Conc HCl, iPrOH, reflux, 2 h; d) Appropriate amine, iPrOH, reflux, 48 h; e) NH₂NH₂.H₂O, EtOH, 0 °C, 30 min; f) TFA, iPrOH, reflux, overnight.
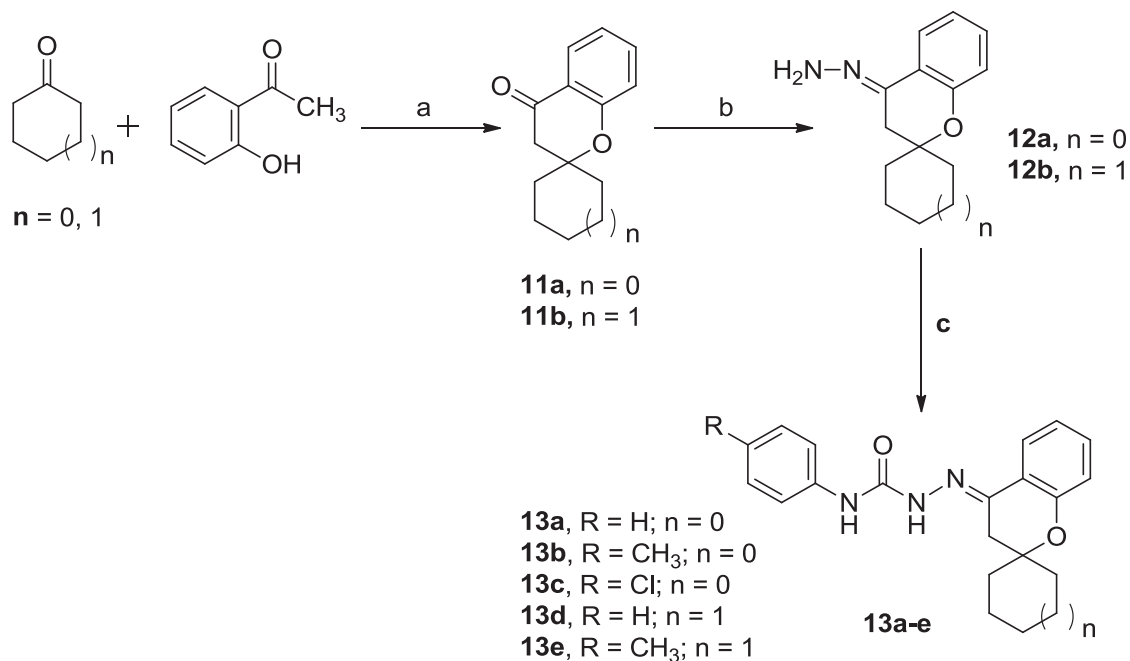
Scheme 2. Reagents and Reaction Conditions: a) Pyrrolidine, MeOH, reflux, 12 h; b) NH₂NH₂.H₂O, EtOH, rt, 3 h; c) Appropriate phenylisocyanate derivative, EtOH, rt, overnight.
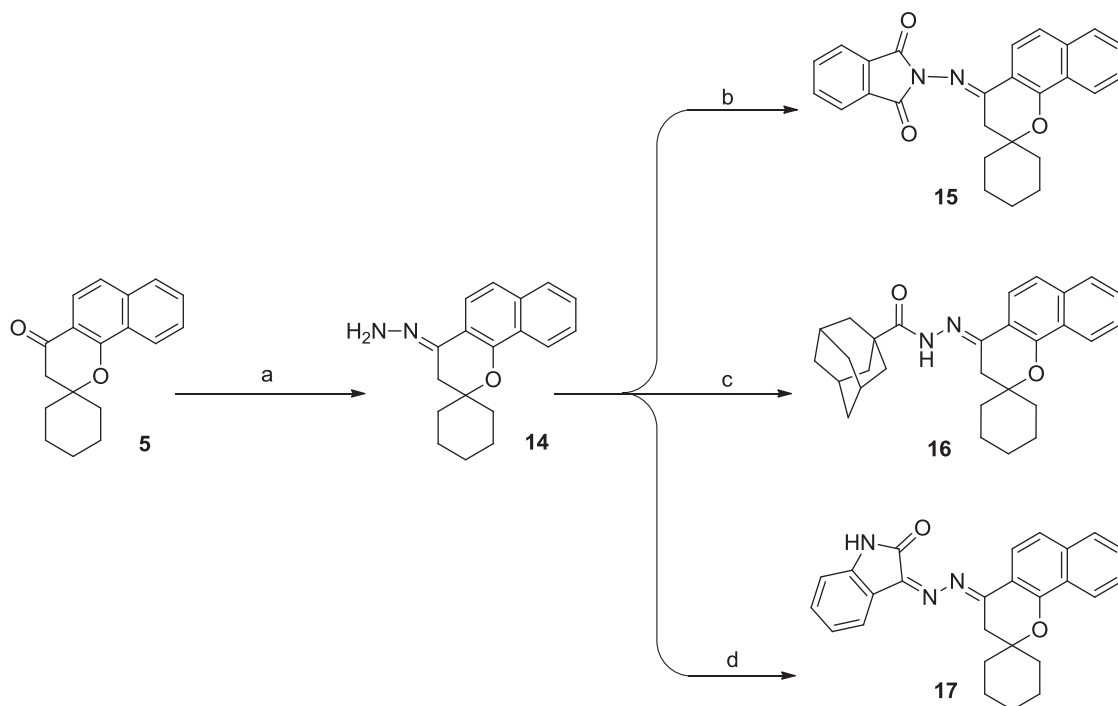
Scheme 3. Reagents and Reaction Conditions: a) NH$_2$NH$_2$.H$_2$O, EtOH, rt, 6 h; b) Phthalic anhydride, anhyd. CH$_3$COONa, gl. AcOH, reflux, overnight; c) Adamantyl carbonyl chloride, TEA, THF, reflux, 2 h; d) Isatin, anhyd. CH$_3$COONa, gl. AcOH, reflux, overnight.

2.2. Pharmacological screening

2.2.1. Anticancer activity

In vitro anticancer activity of the newly synthesized compounds was assessed against three cancer cell lines; MCF-7 (human breast carcinoma), HT-29 (human colorectal adenocarcinoma) and A549 (human lung carcinoma) cell lines using MTT assay [28,29]. The results were summarized in Table 1 and expressed in terms of IC$_{50}$ values, where sorafenib and erlotinib were used as positive controls. The tested compounds showed variable anticancer activities against the three cell lines. Spirochromane derivatives **13** were noticed to be the most common anticancer agents against the three cell lines, if compared to sorafenib (IC$_{50}$ = 3.64, 6.21 and 3.97 μM against MCF-7, A549 and HT-29, respectively) or erlotinib (IC$_{50}$ = 17.32 μM in A549 and IC$_{50}$ > 20 μM in the other cell lines). Compounds **13e** (IC$_{50}$ = 3.09 μM) and **13d** (IC$_{50}$ = 2.15 μM) were the most active against MCF-7 and HT-29 cell lines, respectively. On the other hand, the spirobenzochromene **16** (IC$_{50}$ = 1.78 μM) was the most potent anticancer agent against A549 cell line, followed by compound **13e** (IC$_{50}$ = 2.24 μM). Accordingly, it could be assumed that the anticancer potency of spirochromane derivatives **13c-e** (IC$_{50}$ = 2.15–7.24 μM) dominated over that of bulkier spi-robenzochromene derivatives **8, 10, 14, 15** and **17** (IC$_{50}$ = 3.24–15.07 μM) against the three cell lines tested, except for the adamantyl derivative **16**. However, it could be observed that the semicarbazide derivatives of spirochromane **13** were generally more potent than the thiosemicarbazide or hydrazine derivatives of spirobenzochromenes such as compounds **8f, 10c, 8b** (IC$_{50}$ = 15.07, 14.96, 14.18 μM) on MCF-7, **14, 15** (IC$_{50}$ = 12.87, 12.36 μM) on A549, **14, 8c** (IC$_{50}$ = 9.97, 9.31 μM) on HT-29 cell lines. These two observations gave the rise to the importance of bulkiness effects, in accordance with electronic ones, on the anticancer activity of these compounds. The best anticancer activity amongst compounds **8a-f** was accredited to the *n*-hexyl derivative **8e** (IC$_{50}$ = 3.24 and 3.87 μM against A549 and HT-29, respectively). As for compounds

Table 1
IC$_{50}$ values of the newly synthesized compounds on the cell viability of three cancer cell lines; MCF-7, HT-29 and A549 cell lines.

Comp.	Anticancer activity IC$_{50}$ (μM)[a]		
	MCF-7	A549	HT-29
5	10.65 ± 1.25	10.55 ± 1.07	6.15 ± 0.71
7	5.10 ± 1.31	3.99 ± 0.65	4.13 ± 1.08
8a	13.35 ± 1.74	11.36 ± 1.97	6.77 ± 1.19
8b	14.18 ± 1.61	12.01 ± 1.06	8.34 ± 1.31
8c	11.92 ± 0.97	10.07 ± 1.25	9.31 ± 1.35
8d	11.66 ± 1.03	10.56 ± 1.73	8.17 ± 1.23
8e	4.97 ± 0.42	3.24 ± 0.89	3.87 ± 0.37
8f	15.07 ± 1.29	9.14 ± 0.36	7.44 ± 1.51
10a	11.96 ± 1.18	8.15 ± 1.06	4.74 ± 0.32
10b	9.07 ± 1.10	8.35 ± 0.78	7.09 ± 0.74
10c	14.96 ± 1.27	9.54 ± 0.92	7.37 ± 0.85
13a	12.92 ± 1.71	5.47 ± 1.23	3.11 ± 0.31
13b	7.24 ± 1.36	4.08 ± 0.71	4.71 ± 0.68
13c	4.12 ± 0.98	3.65 ± 1.06	2.75 ± 0.12
13d	3.32 ± 0.77	3.81 ± 0.95	2.15 ± 0.72
13e	3.09 ± 0.11	2.24 ± 0.07	2.44 ± 0.32
14	9.74 ± 0.33	12.87 ± 1.30	9.97 ± 1.24
15	12.06 ± 1.25	12.36 ± 1.87	8.34 ± 1.63
16	4.09 ± 0.21	1.78 ± 0.24	4.45 ± 0.54
17	5.11 ± 0.75	11.12 ± 0.39	7.67 ± 1.07
Sorafenib[b]	3.64 ± 0.78	6.21 ± 0.55	3.97 ± 0.14
Erlotinib[b]	>20	17.32 + 3.11	>20

Three human cancer cell lines were used; MCF-7 (human breast carcinoma), HT-29 (human colorectal adenocarcinoma) and A549 (human lung carcinoma) were treated with the test compounds or vehicle in RPMI media containing 10% FBS for 96 h and cell viability was assessed by MTT assay.
[a] Data are mean ± S.D. (n = 6).
[b] Positive controls.

10a-c, the chlorophenyl derivative **10c** the least potency, against the three cell lines used. Compounds **13a-e** demonstrated better potency in cases of the cycloheptane substitution (**13 d,e**) over the cyclohexane ones (**13a-c**); where the chlorophenyl substituent **13c**

gave the most active derivative amongst the cyclohexane ones. As for compounds **14-17**, the highest anticancer activity was accredited to the adamantly hydrazine derivative of spirobenzochromene **16** against the three cell lines used. The variation in activity amongst the derivatives of each group could be clearly attributed to changeable electronic effects, but the steric effects still could not be neglected when observing activity variations between groups **8, 10, 13** and **14-17**.

2.2.2. Effect on normal cells

Representative compounds **7, 8e, 13e,d, 16** and **17** together with sorafenib were further investigated for their effects on the cell viability of normal fibroblasts (F180) using MTT assay, thus assaying their safety and selectivity profiles. Compounds **7, 16, 17** and sorafenib demonstrated good safety profiles with high IC_{50} values ($IC_{50} > 40 \, \mu M$) on normal fibroblasts. Table 2.

2.2.3. EGFR, B-RAF and tubulin assays

Further mechanistic studies were conducted through investigating the binding affinity of representative active spirochromane and spirobenzo[h]chromene derivatives (**8e**, **13c** and **16**) to EGFR and B-RAF and assaying their effects on tubulin polymerization using suitable positive controls in each assay. The results showed more or less close, yet significant IC_{50} values ($IC_{50} = 1.4$, 1.9 and 1.2 μM on EGFR and 2.7, 2.9 and 2.6 on B-RAF kinase for compounds **8e, 13c** and **16**, respectively), if compared to erlotinib ($IC_{50} = 0.08$ on EGFR and 0.06 μM on B-RAF). These values showed expected higher EGFR affinity than B-RAF kinase. The hydrazine derivative of spirobenzochromenes **16** showed the most potent inhibitory activity against EGFR, suggesting preferential steric and electronic arrangements on EGFR, compared to compounds **8e** and **13c**. Moreover, the three tested compounds showed moderate tubulin polymerization effects, if compared to vincristine and docetaxel. Results were shown in Table 3.

Table 2
IC_{50} values of the most active newly synthesized compounds on the cell viability of the normal fibroblasts (F180).

Comp.	IC_{50} (μM) F180[a]
7	>40
13d	29.87 ± 1.87
8e	31.65 ± 2.03
13e	23.65 ± 1.05
16	>40
17	>40
Sorafenib[b]	>40

Normal fibroblasts (F180 cells) were treated with the test compounds or vehicle in MEM media containing 10% FBS for 96 h and cell viability was assessed by MTT assay.
[a] Data are mean ± S.D. (n = 6).
[b] Positive control.

2.3. Molecular docking study

The present study was performed in an attempt to understand the potency of the newly synthesized spiro compounds and gain some structural insights into their potential binding patterns and possible interactions with both EGFR and B-RAF kinases. Accordingly, the most active spirochromane and spirobenzo[h]chromene derivatives (**8e**, **13c** and **16**) were docked inside the active sites of both EGFR and B-RAF using LIBDOCK embedded in the Discovery Studio software (San Diego, USA). The 3D crystal structures of EGFR (PDB ID: 1M17) and B-RAF (PDB ID: 2FB8), in complex with erlotinib and SB-590885, respectively, were used for this docking simulation study [30–32]. The amino acid residues within a distance of 9 Å around the EGFR and B-RAF co-crystallized ligands in ATP binding pockets were isolated and the possible interactions and ligands orientation were examined. The overlay of the top docking poses EGFR and B-RAF proteins binding pockets were presented in Fig. 2 where the poses **8e**, **13c** and **16** showed good shape complementarity with the ATP-binding sites of both kinases.

Examination of the docking results revealed that the most active compound **8e**, **13c** and **16**, fit nicely inside the ATP-active site engaging in some H-bonds with Met769 and Thr830 residues. In general, it was noticed that the top docked poses adopted a common binding mode where the hydrophobic moieties in the three compounds; p-chlorophenyl, n-hexyl and adamantyl, aligned towards the DFG motif (Asp831, Phe832 and Gly833) with its well-known role in the regulation of kinase activity. Meanwhile, the spirochromane and spirobenzo[h]chromene cores were extended towards the hinge region, forming hydrophobic interactions with Leu694, Val702, Leu768, Cys773, Asp776 and Leu820 amino acid residues, Fig. 3(**A-C**). Compound **13c** was found to bind to EGFR via another one π-cation interaction between p-chlorophenyl ring and Lys721 residue with a distance of 4.3 Å. In addition, the p-chlorophenyl ring in the same compound formed also some other hydrophobic interactions near the DFG motif with Ala719, Met742 and Leu764. Similarly, n-hexyl and adamantyl moieties in compounds **8e** and **16**, respectively formed the same hydrophobic interactions like p-chlorophenyl in compound **13c**. Moreover, compound **16** was found to protrude towards the hinge region to some extent more than the other two compounds, although it showed the most inhibitory activity against the EGFR kinase. Compound **8e** was involved in another H-bond of a distance of 2.2 Å with Thr830 residue. Interestingly, there is a remarkable similarity between the binding pattern of the three docked ligands and that of erlotinib, Fig. 3(D). The 3-ethynylphenyl moiety in erlotinib was located near DFG motif in a similar manner like p-chlorophenyl, n-hexyl and adamantyl moieties forming mostly the same hydrophobic interactions. This apparent similarity between the binding modes of the newly synthesized compounds and the native ligand

Table 3
Effects of compounds on EGFR, B-RAF, and Tubulin Polymerization.

Comp.	IC_{50} ±SEM (μM)[a]		(Tubulin) Effect (Arbitrary units)
	EGFR inhibition	B-RAF inhibition	
8e	1.4 ± 0.8	2.7 ± 1.3	1875 ± 217
13c	1.9 ± 0.7	2.9 ± 1.2	1424 ± 320
16	1.2 ± 0.4	2.6 ± 1.0	1820 ± 290
Erlotinib[b]	0.08 ± 0.04	0.06 ± 0.02	–
Vincristine[b]	–	–	747 ± 205
Docetaxel[b]	–	–	4825 ± 249
DPBS[c]	–	–	2872 ± 214

[a] Data are mean ± S.E. (n = 3).
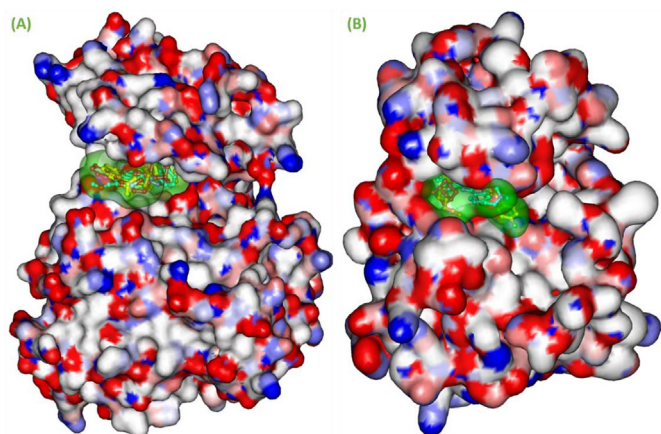[b] Positive controls.
[c] Negative control.

Fig. 2. (A) Overlay of the top docked poses **8e**, **13c** and **16** in addition to the co-crystallized ligand erlotinib into the EGFR kinase binding pocket (PDB code: 1M17); (B) Overlay of the top docked poses **8e**, **13c**, **16** and SB-590885 as a co-crystallized ligand into the B-RAF active site (PDB code: 2FB8). EGFR and B-RAF proteins are represented as a solid surface colored according to atom charges. The binding sites are depicted as transparent green solid surface. (For interpretation of the references to color in this figure legend, the reader is referred to the Web version of this article.)

may greatly contribute to their remarkable potency against the EGFR kinase.

On the other hand, the analysis of the docking results of **8e**, **13c** and **16** into the B-RAF ATP-active pocket indicated that the three shared a similar orientation and disposition inside the active site of B-RAF kinase where the spirochromane and spirobenzo[h]chromene cores were located near the DFG motif (Asp594, Phe595 and Gly596) making several hydrophobic interactions with Ala481,

Val482, Ile527, Val528 and Phe595 residues. Meanwhile, the hydrophobic moieties in the three compounds; *p*-chlorophenyl, n-hexyl and adamantyl, were extended towards the hinge region, forming hydrophobic interactions with Ile463, Cys532, Ser535 and Asn580 amino acid residues, Fig. 4(A–C). In particular, compound **13c** formed a network of three H-bonds with Asn581 and Asp594 residues with distances of 2.6, 2.3 and 2.3 Å, respectively. It was noticed also that the phenyl ring of the spirochromane core was directed towards DFG motif and making a favorable π-stacking interaction with the phenyl ring of Phe583 amino acid. Furthermore, it binds to the active site of B-RAF via one more π-cation interaction between the *p*-chlorophenyl ring and Lys578 residue a distance of 4.5 Å. Regarding compound 8e, the n-hexyl moiety was leaning more towards the bottom of the active site owing to the bulkiness of spirobenzo[h]chromene, which pushed this moiety in a slightly different direction comparing to the *p*-chlorophenyl moiety in **13c** within the kinase hinge region, Fig. 4(B). Additionally, the cyclohexyl ring in compound **8e** was involved in π-stacking interaction with the phenyl ring of Phe583 amino acid residue. Due to the common spirobenzo[h]chromene core present in both compounds **8e** and **16**, they adopted a completely similar binding patterns. Compound **16** was involved in the same hydrophobic interactions like the other docked compounds in addition to one π-stacking interaction with the phenyl ring of Phe583 amino acid residue Fig. 4(c). Comparing the binding patterns of the three docked poses with the co-crystallized ligand, SB-590885, it could be observed the remarkable similarity and complementary between them inside the ATP-binding pocket, Fig. 4(D). It can be concluded that the active site of B-RAF can accommodate both spirochromane and bulkier spirobenzo[h]chromene of the docked poses, however, the bulkier compounds **8e** and **16** showed higher potency than spirochromane derivative **13c**.
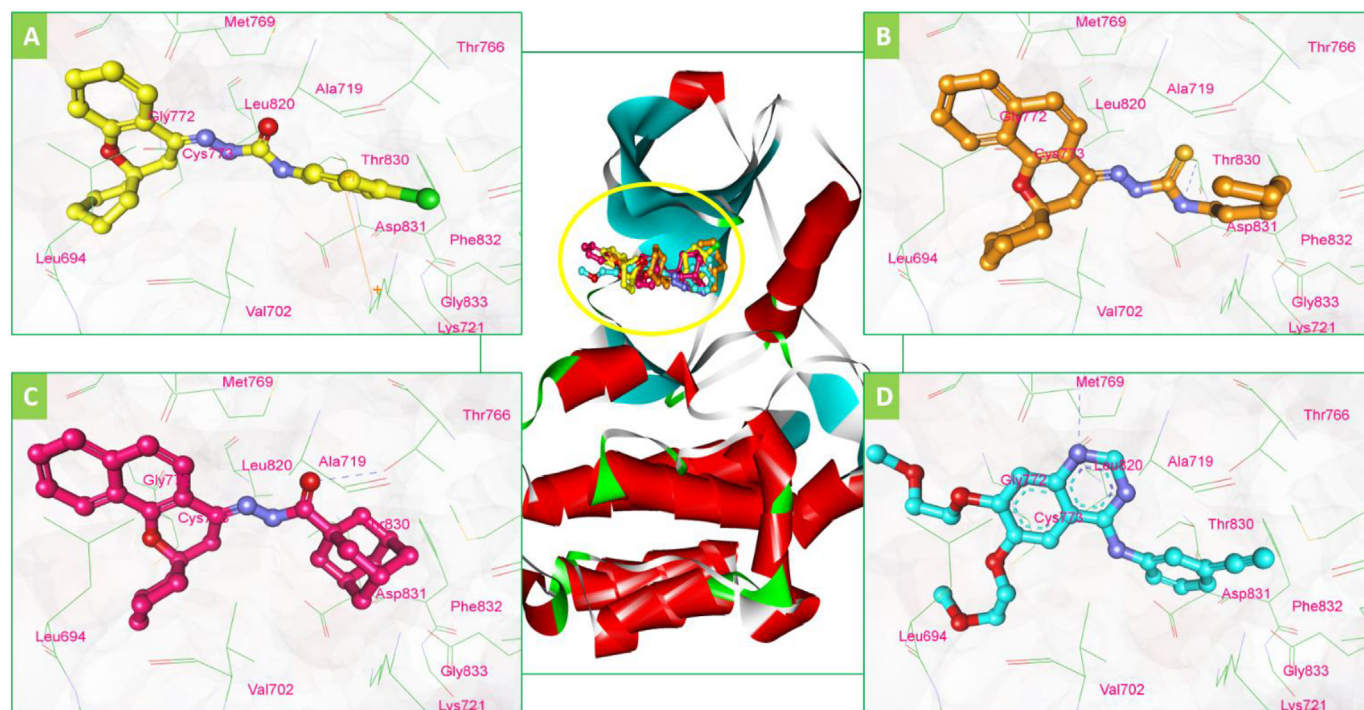

Fig. 3. (A) Docking and binding pattern of compound **13c** (yellow) into ATP-active site of EGFR kinase (PDB code: 1M17); (B) Docking and binding pattern of compound **8e** (orange) into ATP-active site of EGFR kinase; (C) Docking and binding pattern of compound **16** (magenta red) into ATP-active site of EGFR kinase; (D) Docking and binding pattern of erlotinib (cyan) into ATP-active site of EGFR kinase. The superimposition of all docked poses and erlotinib within the ATP-active site of the EGFR protein secondary structure was presented; The poses were rendered as green line models. π-Interactions were represented as a yellow solid line. Hydrogen bonds were represented as dashed blue lines. All hydrogens were removed for the purposes of clarity. (For interpretation of the references to color in this figure legend, the reader is referred to the Web version of this article.)
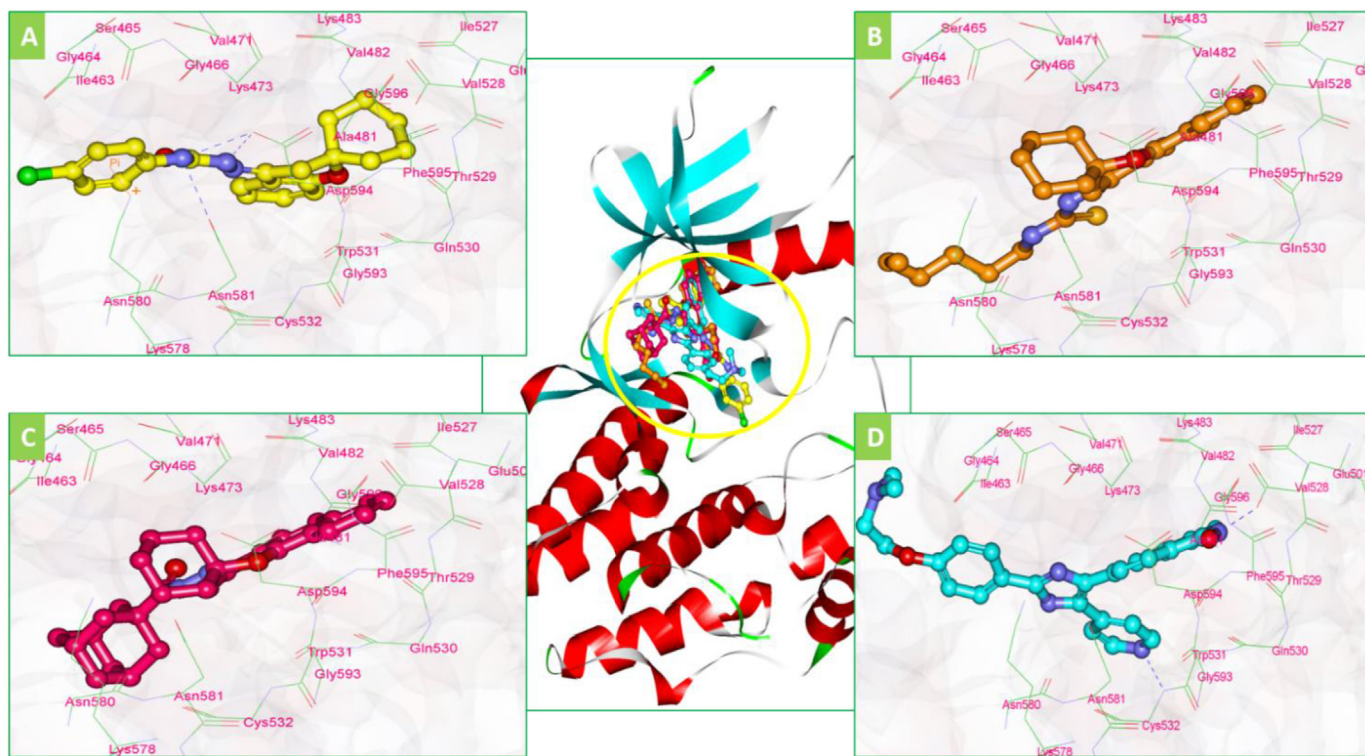
Fig. 4. (A) Docking and binding pattern of compound **13c** (yellow) into ATP-active site of B-RAF kinase (PDB code: 2FB8); (B) Docking and binding pattern of compound 8e (orange) into ATP-active site of B-RAF kinase; (C) Docking and binding pattern of compound **16** (magenta red) into ATP-active site of B-RAF kinase; (D) Docking and binding pattern of **SB-590885** (cyan) into ATP-active site of B-RAF kinase. The superimposition of all docked poses and erlotinib within the ATP-active site of the EGFR protein secondary structure was presented; The poses were rendered as green line models. Hydrogen bonds were represented as dashed blue lines. π-Interactions were represented as a yellow solid line. All hydrogens were removed for the purposes of clarity. (For interpretation of the references to color in this figure legend, the reader is referred to the Web version of this article.)

3. Conclusion

In the present study, a novel series of spirobenzo[*h*]chromene and spirochromane derivatives was synthesized and screened for their anticancer potential against three cancer cell lines. Eight compounds **7**, **8e**, **13a-e** and **16** exhibited better anticancer activity range (IC$_{50}$ = 1.78—5.47 μM) than that of sorafenib (IC$_{50}$ = 3.64—6.21 μM) or erlotinib (IC$_{50}$ > 20 μM). The observed resistance of these cell lines to erlotinib was also reported by many previous studies [33—37]. Thus, the appreciable anticancer activity of our novel compounds in these resistant cell lines is another advantage and promotes their translational promise. Mechanistic study of some representative compounds **8e**, **13c** and **16** was carried out against three anticancer targets; EGFR kinase, B-RAF kinase and Tubulin. The three tested compounds showed better affinity against EGFR than B-RAF kinase. The results showed more or less a close, yet significant IC$_{50}$ values (IC$_{50}$ = 1.4, 1.9 and 1.2 μM on EGFR and 2.7, 2.9 and 2.6 on B-RAF kinase for compounds **8e**, **13c** and **16**, respectively), if compared to erlotinib. The hydrazine derivative of spirobenzochromenes **16** showed the most potent inhibitory activity (IC$_{50}$ = 1.2 μM) against EGFR, suggesting preferential steric and electronic arrangements on EGFR kinase, compared to compounds **8e** and **13c**. Moreover, compounds **8e**, **13c** and **16** showed moderate tubulin polymerization inhibition effects. Molecular docking studies were performed to predict the possible binding patterns of the newly synthesized compounds into the ATP-active sites of EGFR and B-RAF kinases. Together, the docking simulation study, along with the *in vitro* assay results, demonstrated that this class of spiro compounds is promising EGFR and B-RAF dual inhibitors with potential anticancer activity and good leads for further optimization.

4. Experimental protocols

4.1. Chemistry

Chemical reagents and solvents were obtained from commercial sources. Solvents were dried by standard methods when necessary. Elemental analyses were carried out at the microanalytical center in the Faculty of Science, Cairo University. ^{1}H NMR and ^{13}C NMR spectra were recorded with Bruker APX400 spectrometer at 400 MHz and 101 MHz, respectively in DMSO-d_6. Chemical shifts were reported on the δ scale and *J* values were given in Hz. The high-resolution mass spectra (HRMS) were recorded on Agilent 6230 Series Accurate-Mass Time-Of-Flight (TOF) LC/MS. Thin layer chromatography (TLC) was done by silica gel plates 60 GF254, cellulose plates (20 × 20 cm) from Sigma-Aldrich company for chemicals.

4.1.1. Spiro[benzo[h]chromene-2,1′-cyclohexan]-4(3H)-one (**5**) [38,39]

A mixture of cyclohexanone (4.89 g, 0.049 mol), 1′-Hydroxy-2′-Acetonaphthone (9.4 g, 0.049 mol) and pyrrolidine (8.4 mL, 0.10 mol) in anhydrous CH$_3$OH (40 mL) was refluxed overnight. The reaction mixture was then concentrated in vacuo and ethyl acetate (40 mL) was added. The whole mixture was washed with 1 N HCl, brine and dried over Na$_2$SO$_4$. The organic layer was evaporated and hexane (30 mL) was added to the mixture. The resulting precipitate was filtered off and washed with hexane to give pale yellow crystals of compound **5** (75%), mp 162—164 °C. ^{1}H NMR (400 MHz, DMSO-d_6) δ 8.33 (d, *J* = 8.3 Hz, 1H), 7.93 (d, *J* = 8.1 Hz, 1H), 7.71 (m, 2H), 7.64 (t, *J* = 7.6 Hz, 1H), 7.49 (d, *J* = 8.6 Hz, 1H), 2.87 (s, 2H), 2.07 (d, *J* = 14.3 Hz, 2H), 1.78—1.66 (m, 3H), 1.62—1.52 (m, 3H), 1.39—1.22

(m, 2H). ^{13}C NMR (101 MHz, DMSO-d_6) δ 191.96 (C=O), 157.19, 137.61, 130.16, 128.47, 127.12, 125.39, 123.38, 121.45, 120.62, 115.06, 81.63, 47.72, 34.28, 25.17, 21.77. HRMS Calcd. for $C_{18}H_{18}O_2$ [M+H]$^+$ 266.1307, Found 267.1398. Anal. Calcd. for: $C_{18}H_{18}O_2$: C, 81.17; H, 6.81. Found: C, 81.35; H, 6.51.

4.1.2. Methyl hydrazinecarbodithioate (6) [40–42].

A mixture of hydrazine hydrate (6 ml, 0.1 mol) in isopropanol (10 ml) was added slowly with stirring to a cooled solution of KOH (6.6 g, 0.1 M) water (7 ml). Subsequently, CS_2 (10 mL, 0.1 mol) was added dropwise over 1 h to the above ice-cooled solution while the temperature was maintained below 10 °C. The reaction mixture was allowed to stir for another 1 h where a bright yellow color was obtained. At this point, an ice-cooled iodomethane (7 ml, 0.1 mol) was added dropwise over 2 h and the stirring was continued for an additional 1.5 h until the reaction furnished a white precipitate of methyl hydrazinecarbodithioate 6. This precipitate was filtered off, washed with cold water, and recrystallized from dichloromethane to give colorless prism. Yield 51%. m.p. 90–92 °C. HRMS Calcd. for $C_2H_6N_2S_2$ [M+H]$^+$ 121.9972, Found 123.0070.

4.1.3. Methyl 2-(spiro[benzo[h]chromene-2,1′-cyclohexan]-4(3H)-ylidene)hydrazinecarbodithioate (7)

Methyl hydrazinecarbodithioate 6 (0.65 g, 5.39 mmol) was added portionwise to a solution of spiro[benzo[h]chromene-2,1′-cyclohexan]-4(3H)-one 5 (2.0 g, 5.39 mmol) in 40 ml of isopropanol in the presence of a catalytic amount of conc. HCl. The reaction mixture was refluxed for 2 h until a yellow solid began to precipitate. The solid was filtered off and washed with cold isopropanol and air-dried to afford creamy yellow crystals of 3 (77%). ^{1}H NMR (400 MHz, DMSO-d_6) δ 8.31 (d, J = 8.2 Hz, 1H), 7.97 (d, J = 8.1 Hz, 1H), 7.69 (m, 2H), 7.61 (t, J = 7.5 Hz, 1H), 7.47 (d, J = 8.5 Hz, 1H), 6.89 (s, 1H, NH), 2.68 (s, 3H, SCH$_3$), 2.32 (s, 2H), 1.77–1.64 (m, 4H), 1.59–1.51 (m, 4H), 1.21–1.13 (m, 2H). HRMS Calcd. for $C_{20}H_{22}N_2OS_2$ [M+H]$^+$ 370.1174, Found 371.1143. Anal. Calcd. for: $C_{20}H_{22}N_2OS_2$: C, 64.83; H, 5.98; N, 7.56. Found: C, 65.03; H, 6.21; N, 7.84.

4.1.4. General Procedure A for synthesis of compounds (8a-f)

The appropriate amine (0.02 mol) was added to a solution of methyl 2-(spiro[benzo[h]chromene-2,1′-cyclohexan]-4(3H)-yli-dene)hydrazinecarbodithioate 7 (2.4 g, 0.02 mol) in 30 ml iso-propanol and the mixture was refluxed for 48 h until the complete evolution of methyl mercaptan which can be detected by the yellow color produced with moistened Pb(OAc)$_2$ paper. The reaction was also monitored by TLC to confirm its completion. The reaction mixture was then evaporated in vacuo and the resulted precipitate was collected, washed with cold methanol and recrystallized from ethanol to furnish the final compounds 8a-f in good yields.

4.1.5. N′-(spiro[benzo[h]chromene-2,1′-cyclohexan]-4(3H)-ylidene) piperidine-1-carbothiohydrazide (8a)

General Procedure A, yellow solid (63%). ^{1}H NMR (400 MHz, DMSO-d_6) δ 8.24–8.17 (m, 1H), 7.91 (d, J = 8.8 Hz, 1H), 7.88–7.83 (m, 1H), 7.59–7.54 (m, 2H), 7.46 (d, J = 8.8 Hz, 1H), 4.42 (s, 1H, NH), 3.84 (t, J = 7.5 Hz, 4H), 2.96 (s, 2H), 1.97–1.83 (m, 2H), 1.74–1.45 (m, 12H), 1.37–1.18 (m, 2H). ^{13}C NMR (101 MHz, DMSO-d_6) δ 182.55 (C=S), 135.23, 128.22, 128.09, 126.69, 126.48, 126.42, 125.75, 123.37, 122.36, 122.30, 120.71, 77.55, 56.51, 34.58, 26.32, 25.40, 24.40, 21.85, 18.99. HRMS Calcd. for $C_{24}H_{29}N_3OS$ [M+H]$^+$ 407.2031, Found 408.1487. Anal. Calcd. for: $C_{24}H_{29}N_3OS$: C, 70.73; H, 7.17; N, 10.31. Found: C, 70.61; H, 6.99; N, 10.57.

4.1.6. N′-(spiro[benzo[h]chromene-2,1′-cyclohexan]-4(3H)-ylidene) piperazine-1-carbothiohydrazide (8b)

General Procedure A, yellow solid (65%). ^{1}H NMR (400 MHz,

DMSO-d_6) δ 8.26–8.19 (m, 1H), 7.95–7.84 (m, 2H), 7.59–7.52 (m, 2H), 7.47 (d, J = 8.8 Hz, 1H), 4.05 (s, 1H, NH), 3.86–3.75 (m, 4H), 2.97 (s, 1H, NH), 2.83–2.76 (m, 4H), 2.37 (s, 2H), 1.98–1.83 (m, 2H), 1.75–1.44 (m, 6H), 1.40–1.20 (m, 2H). HRMS Calcd. for $C_{23}H_{28}N_4OS$ [M+H]$^+$ 408.1984, Found 409.2132. Anal. Calcd. for: $C_{23}H_{28}N_4OS$: C, 67.61; H, 6.91; N, 13.71. Found: C, 67.84; H, 6.53; N, 13.73.

4.1.7. N′-(spiro[benzo[h]chromene-2,1′-cyclohexan]-4(3H)-ylidene) morpholine-4-carbothiohydrazide (8c)

General Procedure A, dark yellow solid (67%). ^{1}H NMR (400 MHz, DMSO-d_6) δ 8.22 (d, J = 8.2 Hz, 1H), 7.88 (m, 2H), 7.57 (m, 2H), 7.48 (d, J = 8.5 Hz, 1H), 4.40 (s, 1H, NH), 3.90 (t, J = 8.6 Hz, 2H), 3.69 (t, J = 8.6 Hz, 2H), 2.98 (s, 2H), 1.95–1.92 (m, 2H), 1.69–1.67 (m, 4H), 1.56–1.53 (m, 4H), 1.39–1.22 (m, 2H). ^{13}C NMR (101 MHz, DMSO-d_6) δ 183.12 (C=S), 135.32, 133.78, 128.25, 127.76, 126.73, 125.73, 124.90, 122.35, 121.51, 120.61, 78.74, 66.56, 35.69, 34.58, 25.41, 21.84, 19.00. HRMS Calcd. for $C_{23}H_{27}N_3O_2S$ [M+H]$^+$ 409.1824, Found 410.1932. Anal. Calcd. for: $C_{23}H_{27}N_3O_2S$: C, 67.45; H, 6.65; N, 10.26. Found: C, 67.77; H, 6.31; N, 10.49.

4.1.8. 4-Methyl-N′-(spiro[benzo[h]chromene-2,1′-cyclohexan]-4(3H)-ylidene)piperazine-1-carbothiohydrazide (8d)

General Procedure A, yellow solid (68%). ^{1}H NMR (400 MHz, DMSO-d_6) δ 8.22 (d, J = 9.4 Hz, 1H), 7.92–7.85 (m, 2H), 7.56 (m, 2H), 7.47 (d, J = 8.7 Hz, 1H), 4.42 (s, 1H, NH), 3.88 (t, J = 8.4 Hz, 4H), 2.47 (s, 3H), 2.42 (t, J = 8.4 Hz, 4H), 1.91 (s, 2H), 1.61 (m, 8H), 1.36–1.18 (m, 2H). ^{13}C NMR (101 MHz, DMSO-d_6) δ 182.92 (C=S), 135.56, 128.24, 128.16, 127.43, 126.74, 125.74, 123.84, 123.38, 122.41, 122.33, 118.42, 77.59, 56.51, 52.25, 45.98, 43.60, 34.58, 25.41, 21.84, 18.99. HRMS Calcd. for $C_{24}H_{30}N_4OS$ [M+H]$^+$ 422.2140, Found 423.2288. Anal. Calcd. for: $C_{24}H_{30}N_4OS$: C, 68.21; H, 7.16; N, 13.26. Found: C, 68.61; H, 6.97; N, 13.35.

4.1.9. (N-hexyl-2-(spiro[benzo[h]chromene-2,1′-cyclohexan]-4(3H)-ylidene)hydrazinecarbothioamide (8e)

General Procedure A, off-white crystals (63%). ^{1}H NMR (400 MHz, DMSO-d_6) δ 8.64 (s, 1H, NH), 8.29 (d, J = 8.7 Hz, 1H), 8.21 (d, J = 6.9 Hz, 1H), 7.87 (m, 1H), 7.58–7.51 (m, 2H), 7.44 (d, J = 8.8 Hz, 1H), 4.40 (s, 1H, NH), 3.59 (t, J = 8.4 Hz, 2H), 1.88 (s, 2H), 1.72–1.49 (m, 10H), 1.29 (m, 11H). ^{13}C NMR (101 MHz, DMSO-d_6) δ 177.99 (C=S), 150.74, 142.26, 135.26, 128.15, 127.94, 126.49, 125.69, 122.51, 122.27, 120.26, 114.56, 77.41, 56.51, 44.15, 34.68, 31.52, 29.26, 26.54, 22.54, 21.85, 18.99, 14.40. HRMS Calcd. for $C_{25}H_{33}N_3OS$ [M − H]$^+$ 423.2344, Found 422.4500. Anal. Calcd. for: $C_{25}H_{33}N_3OS$: 70.88; H, 7.85; N, 9.92. Found: C, 71.05; H, 7.61; N, 9.99.

4.1.104.1.10. N-cyclohexyl-2-(spiro[benzo[h]chromene-2,1′-cyclohexan]-4(3H)-ylidene)hydrazinecarbothioamide (8f)

General Procedure A, pale yellow solid (61%). ^{1}H NMR (400 MHz, DMSO-d_6) δ 10.28 (s, 1H, NH), 8.19 (d, J = 8.8 Hz, 1H), 8.13 (d, J = 8.6 Hz, 1H), 7.86 (d, J = 6.8 Hz, 1H), 7.59–7.51 (m, 2H), 7.45 (d, J = 8.8 Hz, 1H), 4.47 (s, 1H, NH), 4.29–4.13 (m, 1H), 2.97 (s, 2H), 1.94–1.84 (m, 4H), 1.79–1.42 (m, 12H), 1.34–1.16 (m, 4H). ^{13}C NMR (101 MHz, DMSO-d_6) δ 176.84 (C=S), 150.85, 142.69, 135.28, 128.19, 128.05, 126.57, 125.77, 125.67, 122.29, 120.42, 114.38, 77.44, 56.54, 53.27, 34.65, 32.17, 25.55, 25.37, 21.83, 18.93. HRMS Calcd. for $C_{25}H_{31}N_3OS$ [M+H]$^+$ 421.2188, Found 422.2091. Anal. Calcd. for: $C_{25}H_{31}N_3OS$: C, 71.22; H, 7.41; N, 9.97. Found: C, 71.05; H, 7.61; N, 9.81.

4.1.114.1.11. General procedure B for preparing N-phenylhydrazinecarboxamide (4-phenylsemicarbazide) derivatives (9a-c) [43].

The appropriate phenylisocyanate was added slowly to a cold solution of equimolar amount of hydrazine hydrate in ethanol, The

appropriate phenylisocyanate was added slowly to a cold solution of equimolar amount of hydrazine hydrate in ethanol. The mixture was allowed to stir in ethanol in ice-bath for 1 h. The obtained white precipitate was collected and washed with ethanol. The product was used directly for the next step without any further purification.

4.1.12 4.1.12. N-phenylhydrazinecarboxamide (*9a*)

General Procedure B, white solid (81%). 1H NMR (400 MHz, DMSO-d_6) δ 8.78 (s, 1H, NH), 7.98 (s, 1H, NH), 7.50 (d, J = 8.0 Hz, 2H), 7.26 (t, J = 7.9 Hz, 2H), 6.96 (t, J = 7.4 Hz, 1H). 13C NMR (101 MHz, DMSO-d_6) δ 156.50 (C=O), 140.15, 129.08, 122.30, 118.93.

4.1.13 4.1.13. N-(p-tolyl)hydrazinecarboxamide(*9b*)

General Procedure B, white solid (79%). 1H NMR (400 MHz, DMSO-d_6) δ 8.66 (s, 1H, NH), 7.89 (s, 1H, NH), 7.36 (d, J = 8.2 Hz, 2H), 7.05 (d, J = 8.3 Hz, 2H). 13C NMR (101 MHz, DMSO-d_6) δ 156.56 (C=O), 137.58, 131.05, 129.47, 118.99, 20.79 (CH3).

4.1.14 4.1.14. N-(4-Chlorophenyl)hydrazinecarboxamide (*9b*)

General Procedure B, white solid (77%). 1H NMR (400 MHz, DMSO-d_6) δ 8.97 (s, 1H, NH), 8.31 (s, 1H, NH), 7.89 (d, J = 8.3 Hz, 2H), 7.26 (d, J = 8.3 Hz, 2H). 13C NMR (101 MHz, DMSO-d_6) δ 157.11 (C=O), 137.99, 132.13, 130.65, 119.46.

4.1.15 4.1.15. General procedure C for preparing N-phenyl-2-(spiro [benzo[h]chromene-2,1′-cyclohexan]-4(3H)-ylidene) hydrazinecarboxamide derivatives (*10a-c*)

N-phenylhydrazinecarboxamide derivative **9** (1.88 mmol) was added to a solution of spiro[benzo[*h*]chromene-2,1′-cyclohexan]-4(3*H*)-one **5** (0.5 g, 1.88 mmol) in 40 ml of isopropanol in the presence of a catalytic amount of TFA. The reaction mixture was refluxed for overnight and the organic mixture was concentrated under reduced pressure. The formed solid was filtered off, washed with cold isopropanol and air-dried to afford the final targeted compounds **10a-c** (67−71%).

4.1.16 4.1.16. N-phenyl-2-(spiro[benzo[h]chromene-2,1′-cyclohexan]-4(3H)-ylidene)hydrazinecarboxamide (*10a*)

General Procedure C, yellow solid (69%). ^{1}H NMR (400 MHz, DMSO-d_6) δ 9.89 (s, 1H, NH), 8.33 (d, J = 8.8 Hz, 1H), 7.97 (s, 1H, NH), 7.71 (d, J = 8.6 Hz, 1H), 7.65 (d, J = 7.7 Hz, 3H), 7.57−7.52 (m, 2H), 7.32 (t, J = 7.9 Hz, 2H), 7.04 (t, J = 7.4 Hz, 1H), 2.37 (s, 2H), 1.97−1.88 (m, 1H), 1.75−1.49 (m, 10H), 1.42−1.17 (m, 1H).^{13}C NMR (101 MHz, DMSO-d_6) δ 156.52 (C=O), 146.20, 145.85, 145.75, 140.08, 132.34, 129.11, 128.98, 128.15, 122.39, 121.43, 120.64, 119.00, 118.96, 114.83, 113.39, 73.94, 56.53, 21.91, 18.95. HRMS calcd. for C$_{25}$H$_{25}$N$_3$O$_2$ [M+H]$^+$ 399.1947, Found 400.2048. Anal. Calcd. for: C$_{25}$H$_{25}$N$_3$O$_2$: C, 75.16; H, 6.31; N, 10.52. Found: C, 74.93; H, 6.77; N, 10.37.

4.1.17 4.1.17. 2-(Spiro[benzo[h]chromene-2,1′-cyclohexan]-4(3H)-ylidene)-N-(p-tolyl)hydrazinecarboxamide (*10b*)

General Procedure C, yellow solid (70%). ^{1}H NMR (400 MHz, DMSO-d_6) δ 10.13 (s, 1H, NH), 8.30 (d, J = 8.7 Hz, 1H), 7.87 (s, 1H, NH), 7.69 (d, J = 8.6 Hz, 1H), 7.65 (d, J = 7.6 Hz, 2H), 7.58−7.53 (m, 2H), 7.32−7.23 (m, 2H), 7.11 (d, J = 7.6 Hz, 2H), 2.60 (s, 3H, CH$_3$), 2.31 (s, 2H), 1.93−1.84 (m, 2H), 1.73−1.51 (m, 6H), 1.44−1.10 (m, 2H). HRMS Calcd. for C$_{26}$H$_{27}$N$_3$O$_2$ [M+H]$^+$ 413.2103, Found 414.2586. Anal. Calcd. for: C$_{26}$H$_{27}$N$_3$O$_2$: C, 75.52; H, 6.58; N, 10.16. Found: C, 75.78; H, 6.38; N, 9.83.

4.1.18 4.1.18. N-(4-chlorophenyl)-2-(spiro[benzo[h]chromene-2,1′-cyclohexan]-4(3H)-ylidene)hydrazinecarboxamide (*10c*)

General Procedure C, Off-white solid (62%). ^{1}H NMR (400 MHz, DMSO-d_6) δ 9.88 (s, 1H, NH), 8.31 (d, J = 8.6 Hz, 1H), 7.93 (s, 1H, NH),

7.59 (d, J = 8.6 Hz, 1H), 7.67 (d, J = 7.7 Hz, 2H), 7.60−7.56 (m, 2H), 7.35−7.24 (m, 2H), 7.17 (d, J = 7.7 Hz, 2H), 2.38 (s, 2H), 1.89−1.53 (m, 8H), 1.44−1.10 (m, 2H). HRMS Calcd. for C$_{25}$H$_{24}$ClN$_3$O$_2$ [M+H]$^+$ 433.1557, Found 434.1577. Anal. Calcd. for: C$_{25}$H$_{24}$ClN$_3$O$_2$: C, 69.20; H, 5.57; Cl, 8.17; N, 9.68. Found: C, 69.31; H, 5.90; N, 9.37.

4.1.19 4.1.19. Spiro[chroman-2,1′-cyclohexan]-4-one (*11a*) [34,41]

A mixture of cyclohexanone (4.89 g, 49 mmol), 2-hydroxyacetophenone (6.8 g, 49.8 mmol) and pyrrolidine (8.4 ml, 100 mmol) in methanol (40 ml) was refluxed overnight. The reaction mixture was then concentrated in vacuo and ethyl acetate (40 ml) was added. The whole mixture was washed with 1 N HCl, 1 N NaOH, brine and dried over Na$_2$SO$_4$. The organic layer was evaporated under reduced pressure to give a colorless oil of compound **11a** (83%). HRMS Calcd. for C$_{14}$H$_{16}$O$_2$ [M+H]$^+$ 216.1150, Found 217.1612.

4.1.20 4.1.20. Spiro[chroman-2,1′-cycloheptan]-4-one (*11b*) [26,44]

A mixture of cycloheptanone (5.58 g, 49.8 mmol), 2-hydroxyacetophenone (6.8 g, 49.8 mmol) and pyrrolidine (8.4 ml, 100 mmol) in methanol (40 ml) was refluxed overnight. The reaction mixture was then concentrated in vacuo and ethyl acetate (40 ml) was added. The whole mixture was washed with 1 N HCl, 1 N NaOH, brine and dried over Na$_2$SO$_4$. The organic layer was evaporated under reduced pressure to give a dark yellow oil of compound **11b** (69%). HRMS Calcd. for C$_{15}$H$_{18}$O$_2$ [M+H]$^+$ 230.1307, Found 231.1792.

4.1.21 4.1.21. General procedure D for preparing spiro[chroman-2,1′-cycloalkan]-4-ylidenehydrazine (*12a,b*)

Hydrazine hydrate (3.6 mmol) was added to a solution of spiro [chroman-2,1′-cycloalkan]-4-one **11** (3 mmol) in ethanol (20 ml) and the mixture was left to stir at room temperature for 3 h. The reaction mixture was concentrated in vacuo, water was added and extracted with ethyl acetate (30 ml) and then evaporated under reduced pressure to give a colorless oil from the final intermediates spiro[chroman-2,1′-cycloalkan]-4-ylidenehydrazine **12a,b** in good yields which were used directly for the next step without any further purification.

4.1.22 4.1.22. General procedure E for preparing spiro[chroman-2,1′-cycloalkan]-4-ylidenehydrazine (*13a-c*)

The appropriate phenyl isocyanate derivative (2 mmol) was added to a solution of spiro[chroman-2,1′-cycloalkan]-4-ylidenehydrazine **12a,b** (2 mmol) in ethanol (20 ml). The reaction mixture was allowed to stir at room temperature for overnight. The organic volatiles were removed in vacuo and then water was added. The resulted mixture was extracted using ethyl acetate (40 ml). The organic layer was separated and dried over sodium sulfate and then evaporated under reduced pressure. Petroleum ether was added to the residue to furnish the final compounds **13a-c** in good yields as off-white solids.

4.1.23 4.1.23. N-phenyl-2-(spiro[chroman-2,1′-cyclohexan]-4-ylidene)hydrazinecarboxamide (*13a*)

General Procedure E, Off-white solid (62%). ^{1}H NMR (400 MHz, DMSO-d_6) δ 9.92 (s, 1H, NH), 8.25 (d, J = 7.9 Hz, 1H), 7.65 (d, J = 7.7 Hz, 2H), 7.34−7.21 (m, 3H), 7.03 (t, J = 7.3 Hz, 1H), 6.96 (t, J = 7.5 Hz, 1H), 6.87 (d, J = 8.1 Hz, 1H), 4.35 (s, 1H, NH), 2.83 (s, 2H), 1.80−1.67 (m, 2H), 1.65−1.55 (m, 2H), 1.51 (t, J = 9.8 Hz, 5H), 1.41−1.32 (m, 1H). ^{13}C NMR (101 MHz, DMSO-d_6) δ 154.44 (C=O), 153.99, 140.60, 139.45, 131.27, 128.93, 125.32, 123.03, 121.00, 120.58, 120.53, 118.06, 76.47, 56.50, 34.92, 25.41, 21.66. HRMS Calcd. for C$_{21}$H$_{23}$N$_3$O$_2$ [M+H]$^+$ 349.1790, Found 350.1892. Anal. Calcd. for: C$_{21}$H$_{23}$N$_3$O$_2$: C, 72.18; H, 6.63; N, 12.03. Found: C, 71.93; H, 6.89; N,

11.73.

4.1.244.1.24. 2-(Spiro[chroman-2,1′-cyclohexan]-4-ylidene)-N-(p-tolyl)hydrazinecarboxamide (13b)

General Procedure E, Off-white solid (59%). ^{1}H NMR (400 MHz, DMSO-d_6) δ 9.84 (s, 1H, N$\underline{H}$), 7.51 (d, J = 8.3 Hz, 2H), 7.11 (d, J = 8.2 Hz, 2H), 7.06 (t, J = 6.7 Hz, 1H), 6.95 (t, J = 7.5 Hz, 1H), 6.87 (d, J = 8.2 Hz, 1H), 4.41 (s, 1H, N$\underline{H}$), 2.80 (s, 1H), 2.27 (s, 3H, C$\underline{H}_3$), 1.74–1.70 (m, 2H), 1.60–1.56 (m, 2H), 1.51–1.48 (m, 5H), 1.39–1.21 (m, 1H). ^{13}C NMR (101 MHz, DMSO-d_6) δ 154.40 (C=O), 140.49, 136.82, 131.95, 131.26, 129.75, 129.36, 125.27, 121.02, 120.61, 118.89, 118.06, 76.45, 56.52, 34.89, 25.39, 21.64, 20.86. HRMS Calcd. for $C_{22}H_{25}N_3O_2$ [M+H]$^+$ 363.1947, Found 364.2045. Anal. Calcd. for: $C_{22}H_{25}N_3O_2$: C, 72.70; H, 6.93; N, 11.56. Found: C, 73.03; H, 6.77; N, 11.47.

4.1.254.1.25. N-(4-chlorophenyl)-2-(spiro[chroman-2,1′-cyclohexan]-4-ylidene)hydrazinecarboxamide (13c)

General Procedure E, Off-white solid (61%). ^{1}H NMR (400 MHz, DMSO-d_6) δ 9.99 (s, 1H, NH), 7.72 (d, J = 8.8 Hz, 2H), 7.55 (d, J = 8.8 Hz, 1H), 7.49 (d, J = 8.8 Hz, 1H), 7.36 (d, J = 8.8 Hz, 2H), 6.96 (t, J = 7.5 Hz, 1H), 6.90–6.85 (m, 1H), 4.36 (s, 1H, N$\underline{H}$), 2.83 (s, 2H), 1.77–1.68 (m, 2H), 1.65–1.44 (m, 7H), 1.43–1.29 (m, 1H). ^{13}C NMR (101 MHz, DMSO-d_6) δ 154.48 (C=O), 140.94, 138.55, 131.35, 129.09, 128.75, 126.62, 125.43, 122.05, 120.96, 120.50, 118.06, 76.49, 56.50, 34.90, 25.40, 21.65. HRMS Calcd. for $C_{21}H_{22}ClN_3O_2$ [M+H]$^+$ 383.1401, Found 384.1486. Anal. Calcd. for: $C_{21}H_{22}ClN_3O_2$: C, 65.71; H, 5.78; N, 10.95. Found: C, 65.99; H, 6.01; N, 11.13.

4.1.264.1.26. N-phenyl-2-(spiro[chroman-2,1′-cycloheptan]-4-ylidene)hydrazinecarboxamide (13d)

General Procedure E, Off-white solid (59%). ^{1}H NMR (400 MHz, DMSO-d_6) δ 8.93 (s, 1H, N$\underline{H}$), 7.56 (dd, J = 8.1, 1.4 Hz, 1H), 7.51 (d, J = 7.7 Hz, 2H), 7.31 (t, J = 7.9 Hz, 2H), 7.25 (t, J = 7.7 Hz, 1H), 7.01 (t, J = 7.4 Hz, 1H), 6.91–6.85 (m, 2H), 4.37 (s, 1H, N$\underline{H}$), 2.84 (s, 2H), 2.40–2.37 (m, 4H), 1.89–1.84 (m, 2H), 1.76–1.49 (m, 4H), 1.47–1.18 (m, 2H).^{13}C NMR (101 MHz, DMSO-d_6) δ 158.37 (C=O), 152.42, 150.84, 139.65, 130.74, 129.37, 128.33, 122.73, 120.71, 118.99, 118.81, 117.46, 80.64, 56.50, 29.33, 21.92, 19.02. HRMS Calcd. for $C_{22}H_{25}N_3O_2$ [M+H]$^+$ 363.1947, Found 364.2046. Anal. Calcd. for: $C_{22}H_{25}N_3O_2$: C, 72.70; H, 6.93; N, 11.56. Found: C, 72.58; H, 7.10; N, 11.47.

4.1.274.1.27. 2-(Spiro[chroman-2,1′-cycloheptan]-4-ylidene)-N-(p-tolyl)hydrazinecarboxamide (13e)

General Procedure E, Off-white solid (57%). ^{1}H NMR (400 MHz, DMSO-d_6) δ 9.61 (s, 1H, NH), 7.49 (d, J = 8.1 Hz, 1H), 7.40 (d, J = 7.2 Hz, 4H), 7.18–7.13 (m, 2H), 6.90–6.88 (m, 1H), 4.45 (s, 1H, N$\underline{H}$), 2.80 (s, 2H), 2.37 (s, 3H, C$\underline{H}_3$), 2.33–2.22 (m, 6H), 1.84–1.19 (m, 6H). ^{13}C NMR (101 MHz, DMSO-d_6) δ 156.83 (C=O), 134.56, 131.24, 129.36, 129.11, 126.18, 125.27, 124.81, 124.49, 124.43, 119.17, 117.34, 85.84, 56.52, 37.82, 29.09, 20.99, 18.96. HRMS Calcd. for $C_{23}H_{27}N_3O_2$ [M+H]$^+$ 377.2103, Found 378.2440. Anal. Calcd. for: $C_{23}H_{27}N_3O_2$: C, 73.18; H, 7.21; N, 11.13. Found: C, 72.90; H, 6.99; N, 10.88.

4.1.284.1.28. Spiro[benzo[h]chromene-2,1′-cyclohexan]-4(3H)-ylidenehydrazine (14)

A mixture of hydrazine hydrate (3.6 mmol) and spiro[benzo[h] chromene-2,1′-cyclohexan]-4(3H)-one 5 (3 mmol) in ethanol (20 ml) and a catalytic amount of acetic acid was refluxed for 6 h. The reaction mixture was then concentrated in vacuo and the separated precipitate was filtered off and washed with water to afford the spiro[benzo[h]chromene-2,1′-cyclohexan]-4(3H)-ylidenehydrazine 14 as a yellow solid in good yield. This compound was used directly in the next reaction without any further purification.

4.1.294.1.29. 2-(Spiro[benzo[h]chromene-2,1′-cyclohexan]-4(3H)-ylideneamino)isoindoline-1,3-dione (15)

A mixture of spiro[benzo[h]chromene-2,1′-cyclohexan]-4(3H)-ylidenehydrazine 14 (0.5 g, 1.78 mmol) and phthalic anhydride (0.26 g, 1.78 mmol) and anhydrous sodium acetate (0.19 g, 2.30 mmol) in gl. acetic acid (20 ml) was heated under reflux for overnight. The produced precipitate was collected and washed with water several times to give 2-(spiro[benzo[h]chromene-2,1′-cyclohexan]-4(3H)-ylideneamino)isoindoline-1,3-dione 15 as yellow solid (77%). ^{1}H NMR (400 MHz, DMSO-d_6) δ 8.28–8.16 (m, 4H), 7.91 (d, J = 9.0 Hz, 2H), 7.73–7.36 (m, 4H), 2.90 (s, 2H), 2.04–1.99 (m, 2H), 1.71–1.42 (m, 6H), 1.34–1.17 (m, 2H). HRMS Calcd. for $C_{26}H_{22}N_2O_3$ [M+H]$^+$ 410.1630, Found 411.1680. Anal. Calcd. for: $C_{26}H_{22}N_2O_3$: C, 76.08; H, 5.40; N, 6.82. Found: C, 76.57; H, 5.81; N, 7.03.

4.1.304.1.30. N′-(spiro[benzo[h]chromene-2,1′-cyclohexan]-4(3H)-ylidene)adamantane-1-carbohydrazide (16)

Adamantyl carbonyl chloride (0.46 g, 2.31 mmol) was added to a solution of spiro[benzo[h]chromene-2,1′-cyclohexan]-4(3H)-ylidenehydrazine 14 (0.5 g, 1.78 mmol) in THF (20 ml) in the presence of catalytic amount of triethyl amine. The reaction mixture was heated under reflux for 2 h then it was concentrated under reduced pressure. Water (40 ml) was added and the resulted precipitated was collected. The yellow solid was then crystallized from ethanol to afford compound 16 as yellow solid (63%). ^{1}H NMR (400 MHz, DMSO-d_6) δ 8.34 (d, J = 8.6 Hz, 1H), 8.25 (d, J = 6.9 Hz, 1H), 7.85 (m, 1H), 7.63–7.51 (m, 2H), 7.44 (d, J = 8.6 Hz, 1H), 2.83 (s, 2H), 2.31–2.15 (m, 4H), 1.79–1.62 (m, 10H), 1.59–1.47 (m, 8H), 1.31–1.16 (m, 3H). HRMS Calcd. for $C_{29}H_{34}N_2O_2$ [M+H]$^+$ 442.2620, Found 443.2698. Anal. Calcd. for: $C_{29}H_{34}N_2O_2$: C, 78.70; H, 7.74; N, 6.33. Found: C, 78.62; H, 8.05; N, 6.47.

4.1.314.1.31. 3-((E)-spiro[benzo[h]chromene-2,1′-cyclohexan]-4(3H)-ylidenehydrazono)indolin-2-one (17)

A mixture of spiro[benzo[h]chromene-2,1′-cyclohexan]-4(3H)-ylidenehydrazine 14 (0.5 g, 1.78 mmol) and isatin (0.26 g, 1.78 mmol) and anhydrous sodium acetate (0.19 g, 2.30 mmol) in gl. acetic acid (20 ml) was heated under reflux for overnight. The reaction mixture was allowed to cool and then poured into ice-water (100 ml). The formed precipitate was collected and washed with water to afford 3-((E)-Spiro[benzo[h]chromene-2,1′-cyclohexan]-4(3H)-ylidenehydrazono)indolin-2-one 17 as dark yellow solid (73%). ^{1}H NMR (400 MHz, DMSO-d_6) δ 8.81 (s, 1H, N$\underline{H}$), 8.35–8.13 (m, 4H), 7.91–7.65 (m, 2H), 7.45–7.21 (m, 4H), 2.87 (s, 2H), 1.98–1.90 (m, 2H), 1.82–1.51 (m, 6H), 1.39–1.08 (m, 2H). HRMS Calcd. for $C_{26}H_{23}N_3O_2$ [M+H]$^+$ 409.1790, Found 410.1933. Anal. Calcd. for: $C_{26}H_{23}N_3O_2$: C, 76.26; H, 5.66; N, 10.26. Found: C, 75.97; H, 5.31; N, 10.45.

4.2. Biological screening

4.2.1. Cell Culture

The used cancer cell lines in this study; MCF-7 (human breast carcinoma), HT-29 (human colorectal adenocarcinoma) and A549 (human lung carcinoma) were obtained from European Collection of Cell Cultures (ECACC, UK). The normal fibroblasts (F180) were kindly provided by professor Ekkehard Dikomey (University Cancer Center, Hamburg University, Hamburg, Germany). Cancer cell lines were cultured in Roswell Park Memorial Institute medium (RPMI, Sigma-Aldrich, St. Louis, MO, USA) while the fibroblast cells were maintained in Minimum Essential Media (MEM). All media were supplemented with 10% fetal bovine serum (FBS, Sigma-Aldrich) and 1% penicillin/streptomycin (Sigma-Aldrich). All incubations were done at 37 °C in a humidified atmosphere of 5% CO_2.

4.2.2. Cell viability analysis

Cell viability was assessed using the 3-(4,5-dimethylthiazol-2-yl)-2,5-diphenyltetrazolium bromide (MTT) assay as described before assay [28,29]. In brief, cancer cells or normal fibroblast cells (F180) were seeded at 4×10^4 per well density in 96 well flat-bottomed plates, and incubated in 10% FBS— supplemented media. After 24 h of seeding, the cells were treated with different concentrations of test compounds, sorafenib or erlotinib. The vehicle (DMSO) was used as a negative control. Following 96 h of treatment, the media were aspirated and replaced by 200 μL the same media containing 0.5 mg/ml of MTT tetrazolium dye (Sigma-Aldrich) and incubated for 2 h at 37 °C. The MTT-containing media were then aspirated and the formed formazan crystals were solubilized in 200 μl of DMSO per well. Absorbance was measured at 570 nm using a microplate reader (Thermo Scientific).

4.2.3. Tubulin polymerization assay

The activity of compounds on tubulin polymerization was investigated using Tubulin Polymerization Assay Kit (Cytoskeleton Inc., Denver, CO, USA), which works via fluorescent reporter enhancement [45]. The fluorescence of the compounds (dissolved in DMSO at 5 and 25 μM concentration) was recorded in triplicates using FLUO star OPTIMA. Docetaxel and vincristine (Apoteket AB, Sweden) served as positive stabilizing and destabilizing controls. Both were used at 3 μM concentration in PBS [46].

4.2.4. EGFR inhibitory assay

Baculoviral expression vectors such as pFASTBacHTc and pBlueBacHis2B were separately used to clone 1.6 kb cDNA encoding EGFR cytoplasmic domain (EGFR-CD, amino acids 645—1186) with His6 tag. Sf-9 cells were infected with the vectors to express the protein and cell pellets were collected 3 days post infection. Cell pellets were processed essentially as detailed before [47]. On the basis of Dissociation-Enhanced Lanthanide Fluorescence Immunoassay/Time-Resolved Fluorometry, EGFR kinase assay was performed to measure the level of auto-phosphorylation. DMSO (100%) was used to dissolve the compounds, followed by dilution to suitable concentrations using 25 mM HEPES at pH 7.4. In every well, 10 μL (5 ng for EGFR) recombinant enzyme (1:80 dilution in 100 mM HEPES) was incubated with 10 μL compound at 25 °C for 10 min, followed by the addition of 10 μL 5X buffer (containing 1 mM DTT, 100 μM Na_3VO_4, 2 mM $MnCl_2$ and 20 mM HEPES) and 20 μL 0.1 mM ATP-50 mM $MgCl_2$ for 1 h. By incubating the enzyme with or without ATP-$MgCl_2$, positive and negative controls were included in every plate. After incubation, the liquid was removed, and wash buffer was used to wash the plates thrice. To each well of the plate, 75 μL (400 ng) europium-labeled antiphosphotyrosine antibody was added for another 1 h, followed by washing. After adding the enhancement solution, the signal was detected (with excitation and emission at 340 at 615 nm, respectively) using Victor (Wallac Inc.). The following equation was used to calculate the autophosphorylation inhibition (%) by the compounds:

$$100\% - [(negative\ control)/(positive\ control) - (negative\ control) \\ \times]$$

The IC_{50} was calculated using the curves of inhibition (%) with eight concentrations of the compound. Most of the signal detected by antiphosphotyrosine antibody is from EGFR, as the impurities in the enzyme preparation are quite low.

4.2.5. B-RAF kinase assay

Test compounds were subjected to V600E mutant B-RAF kinase assay in triplicate. 1 μL drug and 4 μL assay dilution buffer were pre-incubated with 7.5 ng mouse full-length GST-tagged B-RAF^{V600E} (Invitrogen, PV3849) at 25 °C for 1 h. The assay was started by adding 5 μL solution comprising 200 ng recombinant human full length, *N*-terminal His-tagged MEK1 (Invitrogen), 30 mM $MgCl_2$ and 200 μM ATP in the assay dilution buffer, followed by continuation at 25 °C for 25 min. Using 5X protein denaturing buffer (LDS) solution (5 μL), the assay was quenched. Further denaturing of protein was performed by heating at 70 °C for 5 min. Electrophoresis was performed at 200 V by loading 10 μL of each reaction into a 15-well 4—12% precast NuPage gel plate (Invitrogen). Once the electrophoresis was finished, the front (containing additional hot ATP) was cut from the gel and subsequently discarded. A phosphor screen was used to develop the dried gel. A reaction containing no inhibitor was used as positive control, whereas a reaction without active enzyme served as negative control.

4.3. Molecular docking study

The docking simulation was performed using LIBDOCK protocol embedded in the Discovery Studio Software (San Diego, USA). The 3D structures of EGFR and B-RAF (PDB codes; 1M17 and 2FB8), respectively, were downloaded from Protein Data Bank (PDB) website, prepared, cleaned and the H-atoms were added. The binding pockets were defined as spheres of the selected co-crystallized ligands, erlotinib and SB-590885. Furthermore, all bound water molecules were eliminated from the used 3D protein structure before the docking process. The ligand minimization tool was used for minimizing the structure of the compounds with CHARMm ForceField. The Number of polar or apolar receptor hotspots for conformer matching was set to 100. Moreover, the docking tolerance (RMSD tolerance) value of 0.25 Å was employed to accept or reject any given match. The High Quality mode was selected from different LibDock modes to perform this docking study. The algorithm for generating conformations was set to FAST to quickly provide a set of diverse low-energy conformations. Finally, the top-docked poses were selected according to the Lib-DockScore to be examined.

Appendix A. Supplementary data

Supplementary data related to this article can be found at https://doi.org/10.1016/j.ejmech.2018.03.001.

References

[1] L.A. Torre, F. Bray, R.L. Siegel, J. Ferlay, J. Lortet-Tieulent, A. Jemal, Global cancer statistics, 2012, CA Cancer J. Clin. 65 (2015) 87—108.

[2] H.A. Omar, A.M. Sargeant, J.R. Weng, D. Wang, S.K. Kulp, T. Patel, C.S. Chen, Targeting of the Akt-nuclear factor-kappa B signaling network by [1-(4-chloro-3-nitrobenzenesulfonyl)-1H-indol-3-yl]-methanol (OSU-A9), a novel indole-3-carbinol derivative, in a mouse model of hepatocellular carcinoma, Mol. Pharmacol. 76 (2009) 957—968.

[3] G. Housman, S. Byler, S. Heerboth, K. Lapinska, M. Longacre, N. Snyder, S. Sarkar, Drug resistance in cancer: an overview, Cancers 6 (2014) 1769—1792.

[4] C. Holohan, S. Van Schaeybroeck, D.B. Longley, P.G. Johnston, Cancer drug resistance: an evolving paradigm, Nat. Rev. Canc. 13 (2013) 714—726.

[5] L. Xie, P.E. Bourne, Developing multi-target therapeutics to fine-tune the evolutionary dynamics of the cancer ecosystem, Front. Pharmacol. 6 (2015) 209.

[6] S.M. Abdin, D.M. Zaher, E.A. Arafa, H.A. Omar, Tackling cancer resistance by immunotherapy: updated clinical impact and safety of PD-1/PD-L1 inhibitors, Cancers 10 (2018).

[7] G. Cassinelli, V. Zuco, L. Gatti, C. Lanzi, N. Zaffaroni, D. Colombo, P. Perego, Targeting the Akt kinase to modulate survival, invasiveness and drug resistance of cancer cells, Curr. Med. Chem. 20 (2013) 1923—1945.

[8] S.J. Baker, E.P. Reddy, Targeted inhibition of kinases in cancer therapy, Mt. Sinai J. Med. 77 (2010) 573—586.

[9] M.J. Akhtar, A.A. Siddiqui, A.A. Khan, Z. Ali, R.P. Dewangan, S. Pasha, M.S. Yar, Design, synthesis, docking and QSAR study of substituted benzimidazole linked oxadiazole as cytotoxic agents, EGFR and erbB2 receptor inhibitors, Eur.

J. Med. Chem. 126 (2017) 853–869.

[10] T. Regad, Targeting RTK signaling pathways in cancer, Cancers 7 (2015) 1758–1784.

[11] S. Wang, Y. Song, D. Liu, EAI045: the fourth-generation EGFR inhibitor overcoming T790M and C797S resistance, Cancer. Lett 385 (2017) 51–54.

[12] W. Yang, Y. Chen, X. Zhou, Y. Gu, W. Qian, F. Zhang, W. Han, T. Lu, W. Tang, Design, synthesis and biological evaluation of bis-aryl ureas and amides based on 2-amino-3-purinylpyridine scaffold as DFG-out B-Raf kinase inhibitors, Eur. J. Med. Chem. 89 (2015) 581–596.

[13] H.A. Omar, M.F. Tolba, J.H. Hung, T.H. Al-Tel, OSU-2S/Sorafenib synergistic antitumor combination against hepatocellular carcinoma: the role of PKCdelta/p53,, Front. Pharmacol. 7 (2016) 463.

[14] S.I. El-Desoky, F.A. Badria, M.A. Abozeid, E.A. Kandeel, A.H. Abdel-Rahman, Synthesis and antitumor studies of novel benzopyrano-1,2,3-selenadiazole and spiro[benzopyrano]-1,3,4-thiadiazoline derivatives, Med. Chem. Res. 22 (2013) 2105–2114.

[15] M. Mujahid, P. Yogeeswari, D. Sriram, U.M.V. Basavanag, E. Diaz-Cervantes, L. Cordoba-Bahena, J. Robles, R.G. Gonnade, M. Karthikeyan, R. Vyas, M. Muthukrishnan, Spirochromone-chalcone conjugates as antitubercular agents: synthesis, bio evaluation and molecular modeling studies, RSC Adv. 5 (2015) 106448–106460.

[16] L. Feng, M.M. Maddox, M.Z. Alam, L.S. Tsutsumi, G. Narula, D.F. Bruhn, X. Wu, S. Sandhaus, R.B. Lee, C.J. Simmons, Y.C. Tse-Dinh, J.G. Hurdle, R.E. Lee, D. Sun, Synthesis, structure-activity relationship studies, and antibacterial evaluation of 4-chromanones and chalcones, as well as olympicin A and derivatives, J. Med. Chem. 57 (2014) 8398–8420.

[17] R.R. Dandu, J.A. Lyons, R. Raddatz, Z. Huang, L.D. Aimone, R.L. Hudkins, Synthesis and evaluation of a new series of 1'-cyclobutyl-6-(4-piperidyloxy)spiro [benzopyran-2,4'-piperidine] derivatives as high affinity and selective histamine-3 receptor (H3R) antagonists, Bioorg. Med. Chem. Lett 22 (2012) 2151–2153.

[18] T. Huang, J. Sun, Q. Wang, J. Gao, Y. Liu, Synthesis, Biological Evaluation and Molecular Docking Studies of piperidinylpiperidines and spirochromanones possessing quinoline moieties as acetyl-CoA carboxylase inhibitors, Molecules 20 (2015) 16221–16234.

[19] Y. Uto, Y. Ueno, Y. Kiyotsuka, Y. Miyazawa, H. Kurata, T. Ogata, M. Yamada, T. Deguchi, M. Konishi, T. Takagi, S. Wakimoto, J. Ohsumi, Synthesis and evaluation of novel stearoyl-CoA desaturase 1 inhibitors: 1'-{6-[5-(pyridin-3-ylmethyl)-1,3,4-oxadiazol-2-yl]pyridazin-3-yl}-3,4-dihydrospi ro[chromene-2,4'-piperidine] analogs, Eur. J. Med. Chem. 45 (2010) 4788–4796.

[20] M. Varasi, F. Thaler, A. Abate, C. Bigogno, R. Boggio, G. Carenzi, T. Cataudella, R. Dal Zuffo, M.C. Fulco, M.G. Rozio, A. Mai, G. Dondio, S. Minucci, C. Mercurio, Discovery, synthesis, and pharmacological evaluation of spiropiperidine hydroxamic acid based derivatives as structurally novel histone deacetylase (HDAC) inhibitors, J. Med. Chem. 54 (2011) 3051–3064.

[21] K. Krishnan, K. Prathiba, V. Jayaprakash, A. Basu, N. Mishra, B. Zhou, S. Hu, Y. Yen, Synthesis and ribonucleotide reductase inhibitory activity of thio-semicarbazones, Bioorg. Med. Chem. Lett 18 (2008) 6248–6250.

[22] F. Thaler, L. Moretti, R. Amici, A. Abate, A. Colombo, G. Carenzi, M.C. Fulco, R. Boggio, G. Dondio, S. Gagliardi, S. Minucci, L. Sartori, M. Varasi, C. Mercurio, Synthesis, biological characterization and molecular modeling insights of spirochromanes as potent HDAC inhibitors, Eur. J. Med. Chem. 108 (2016) 53–67.

[23] B.F. Roberts, I.D. Iyamu, S. Lee, E. Lee, L. Ayong, D.E. Kyle, Y. Yuan, R. Manetsch, D. Chakrabarti, Spirocyclic chromanes exhibit antiplasmodial activities and inhibit all intraerythrocytic life cycle stages, Int. J. Parasitol. Drugs Drug. Resist 6 (2016) 85–92.

[24] B. Le Bourdonnec, R.T. Windh, L.K. Leister, Q.J. Zhou, C.W. Ajello, M. Gu, G.H. Chu, P.A. Tuthill, W.M. Barker, M. Koblish, D.D. Wiant, T.M. Graczyk, S. Belanger, J.A. Cassel, M.S. Feschenko, B.L. Brogdon, S.A. Smith, M.J. Derelanko, S. Kutz, P.J. Little, R.N. DeHaven, D.L. DeHaven-Hudkins, R.E. Dolle, Spirocyclic delta opioid receptor agonists for the treatment of pain: discovery of N,N-diethyl-3-hydroxy-4-(spiro[chromene-2,4'-piperidine]-4-yl) benzamide (ADL5747), J. Med. Chem. 52 (2009) 5685–5702.

[25] S.M. Atta, D.S. Farrag, A.M. Sweed, A.H. Abdel-Rahman, Preparation of new polycyclic compounds derived from benzofurans and furochromones. An approach to novel 1,2,3-thia-, and selena-diazolofurochromones of antici-pated antitumor activities, Eur. J. Med. Chem. 45 (2010) 4920–4927.

[26] H.J. Kabbe, Eine einfache Synthese von 4-Chromanonen, Synthesis (1978) 886–887, 1978.

[27] D.C. Greenbaum, Z. Mackey, E. Hansell, P. Doyle, J. Gut, C.R. Caffrey, J. Lehrman, P.J. Rosenthal, J.H. McKerrow, K. Chibale, Synthesis and structure-activity relationships of parasiticidal thiosemicarbazone cysteine protease inhibitors against Plasmodium falciparum, Trypanosoma brucei, and Trypanosoma cruzi, J. Med. Chem. 47 (2004) 3212–3219.

[28] J.R. Weng, L.Y. Bai, H.A. Omar, A.M. Sargeant, C.T. Yeh, Y.Y. Chen, M.H. Tsai, C.F. Chiu, A novel indole-3-carbinol derivative inhibits the growth of human oral squamous cell carcinoma in vitro, Oral Oncol. 46 (2010) 748–754.

[29] A.H. Abdelazeem, A.M. Gouda, H.A. Omar, M.F. Tolba, Design, synthesis and biological evaluation of novel diphenylthiazole-based cyclooxygenase inhibitors as potential anticancer agents, Bioorg. Chem. 57 (2014) 132–141.

[30] J. Stamos, M.X. Sliwkowski, C. Eigenbrot, Structure of the epidermal growth factor receptor kinase domain alone and in complex with a 4-anilinoquinazoline inhibitor, J. Biol. Chem. 277 (2002) 46265–46272.

[31] A.J. King, D.R. Patrick, R.S. Batorsky, M.L. Ho, H.T. Do, S.Y. Zhang, R. Kumar, D.W. Rusnak, A.K. Takle, D.M. Wilson, E. Hugger, L. Wang, F. Karreth, J.C. Lougheed, J. Lee, D. Chau, T.J. Stout, E.W. May, C.M. Rominger, M.D. Schaber, L. Luo, A.S. Lakdawala, J.L. Adams, R.G. Contractor, K.S. Smalley, M. Herlyn, M.M. Morrissey, D.A. Tuveson, P.S. Huang, Demonstration of a genetic therapeutic index for tumors expressing oncogenic BRAF by the kinase inhibitor SB-590885, Cancer.Res 66 (2006) 11100–11105.

[32] A.H. Abdelazeem, M.T. El-Saadi, E.G. Said, B.G.M. Youssif, H.A. Omar, S.M. El-Moghazy, Novel diphenylthiazole derivatives with multi-target mechanism: synthesis, docking study, anticancer and anti-inflammatory activities, Bioorg. Chem. 75 (2017) 127–138.

[33] T. Li, Y.H. Ling, I.D. Goldman, R. Perez-Soler, Schedule-dependent cytotoxic synergism of pemetrexed and erlotinib in human non-small cell lung cancer cells, Clin. Cancer. Res: An Official Journal of the American Association for Cancer Research 13 (2007) 3413–3422.

[34] I. Kritikou, E. Giannopoulou, A.K. Koutras, V.T. Labropoulou, H.P. Kalofonos, The combination of antitumor drugs, exemestane and erlotinib, induced resistance mechanism in H358 and A549 non-small cell lung cancer (NSCLC) cell lines, Pharm. Biol. 52 (2013) 444–452.

[35] M. Orzaez, T. Guevara, M. Sancho, E. Perez-Paya, Intrinsic caspase-8 activation mediates sensitization of erlotinib-resistant tumor cells to erlotinib/cell-cycle inhibitors combination treatment, Cell Death Dis. 3 (2012) e415.

[36] F. Yamasaki, D. Zhang, C. Bartholomeusz, T. Sudo, G.N. Hortobagyi, K. Kurisu, N.T. Ueno, Sensitivity of breast cancer cells to erlotinib depends on cyclin-dependent kinase 2 activity, Mol.Cancer.Ther 6 (2007) 2168–2177.

[37] E. Buck, A. Eyzaguirre, E. Brown, F. Petti, S. McCormack, J.D. Haley, K.K. Iwata, N.W. Gibson, G. Griffin, Rapamycin synergizes with the epidermal growth factor receptor inhibitor erlotinib in non-small-cell lung, pancreatic, colon, and breast tumors, Mol.Cancer.Ther. 5 (2006) 2676–2684.

[38] H.-J. Kabbe, A. Widdig, Synthesis and reactions of 4-chromanones, Angew Chem Int Ed 21 (1982) 247–256.

[39] M.I. Hegab, A.E. Rashad, A.H. Shamroukh, I.A. Hamza, Synthesis and deriva-tization of angular 3-chloro-3-chlorosulfenyl naphtho[1,2-b]pyran(4H)-4-ones with evaluation of antiviral activity, J. Sulfur Chem. 27 (2006) 213–224.

[40] D.L. Klayman, J.F. Bartosevich, T.S. Griffin, C.J. Mason, J.P. Scovill, 2-Acetylpyridine thiosemicarbazones. 1. A new class of potential antimalarial agents, J. Med. Chem. 22 (1979) 855–862.

[41] T. Stringer, D. Taylor, C. de Kock, H. Guzgay, A. Au, S.H. An, B. Sanchez, R. O'Connor, N. Patel, K.M. Land, P.J. Smith, D.T. Hendricks, T.J. Egan, G.S. Smith, Synthesis, characterization, antiparasitic and cytotoxic evaluation of thioureas conjugated to polyamine scaffolds, Eur. J. Med. Chem. 69 (2013) 90–98.

[42] M.A.F.A. Manan, M.I.M. Tahir, K.A. Crouse, F.N.-F. How, D.J. Watkin, Synthesis, characterization and antibacterial activity of schiff base derived from S-Methyldithiocarbazate and methylisatin, J. Chem. Crystallogr. 42 (2012) 173–179.

[43] S.F. Asghar, K.A. Yasin, S. Aziz, Synthesis and cyclisation of 1,4-disubstituted semicarbazides, Nat. Prod. Res. 24 (2010) 315–325.

[44] U.M. Battisti, C. Corrado, C. Sorbi, A. Cornia, A. Tait, D. Malfacini, M.C. Cerlesi, G. Calo, L. Brasili, Synthesis, enantiomeric separation and docking studies of spiropiperidine analogues as ligands of the nociceptin/orphanin FQ receptor, MedChemComm 5 (2014) 973–983.

[45] D. Bonne, C. Heusele, C. Simon, D. Pantaloni, 4',6-Diamidino-2-phenylindole, a fluorescent probe for tubulin and microtubules, J. Biol. Chem. 260 (1985) 2819–2825.

[46] D.J. Slamon, W. Godolphin, L.A. Jones, J.A. Holt, S.G. Wong, D.E. Keith, W.J. Levin, S.G. Stuart, J. Udove, A. Ullrich, et al., Studies of the HER-2/neu proto-oncogene in human breast and ovarian cancer, Science 244 (1989) 707–712.

[47] Y. Luo, Y. Li, K.M. Qiu, X. Lu, J. Fu, H.L. Zhu, Metronidazole acid acyl sulfon-amide: a novel class of anticancer agents and potential EGFR tyrosine kinase inhibitors, Bioorg. Med. Chem. 19 (2011) 6069–6076.